OPEN ACCESS

KING'S College LONDON

King's Research Portal

DOI:
10.1523/JNEUROSCI.1456-18.2018

Document Version
Peer reviewed version

Link to publication record in King's Research Portal

Citation for published version (APA):
Prekop, H.-T., Kroiss, A., Rook, V., Zagoraiou, L., Jessell, T., Fernandes, C., Delogu, A., & Wingate, R. J. T. (2018). Sox14 is required for a specific subset of cerebello–olivary projections. *Journal of Neuroscience*, *38*(44), 9539-9550. https://doi.org/10.1523/JNEUROSCI.1456-18.2018

Citing this paper
Please note that where the full-text provided on King's Research Portal is the Author Accepted Manuscript or Post-Print version this may differ from the final Published version. If citing, it is advised that you check and use the publisher's definitive version for pagination, volume/issue, and date of publication details. And where the final published version is provided on the Research Portal, if citing you are again advised to check the publisher's website for any subsequent corrections.

General rights
Copyright and moral rights for the publications made accessible in the Research Portal are retained by the authors and/or other copyright owners and it is a condition of accessing publications that users recognize and abide by the legal requirements associated with these rights.

•Users may download and print one copy of any publication from the Research Portal for the purpose of private study or research.
•You may not further distribute the material or use it for any profit-making activity or commercial gain
•You may freely distribute the URL identifying the publication in the Research Portal

Take down policy
If you believe that this document breaches copyright please contact librarypure@kcl.ac.uk providing details, and we will remove access to the work immediately and investigate your claim.

Download date: 05. Jan. 2025

SOX14 IS REQUIRED FOR A SPECIFIC SUBSET OF CEREBELLO-OLIVARY PROJECTIONS

Hong Ting Prekop [1,2], Anna Kroiss [1], Victoria Rook [2], Laskaro Zagoraiou [3,4], Thomas Jessell [4], Cathy Fernandes [5], Alessio Delogu [1*], Richard Wingate [2*]

1. Department of Basic and Clinical Neuroscience, King's College London
2. MRC Centre for Neurodevelopmental Disorders, King's College London, SE1 1UL
3. Biomedical Research Foundation Academy Of Athens
4. Department of Neuroscience, Columbia University
5. Centre for Social, Genetic and Developmental Psychiatry, King's College London

* Joint corresponding authors to whom correspondence should be addressed

Alessio.delogu@kcl.ac.uk

Richard.wingate@kcl.ac.uk

Submitting author: Dr Richard Wingate, MRC Centre for Neurodevelopmental Disorders, 4th floor

New Hunts House, Guy's Campus King's College London, SE1 1UL, UK

Richard.wingate@kcl.ac.uk

Pages: 33

Figures: 6

Abstract (250): 149

Introduction (650): 675

Discussion (1500): 1421

ACKNOWLEDGMENTS

This work was supported by BBSRC grant BB/L020068/1 to A.D. and a NIHR Maudsley Biomedical Research Centre PhD studentship to H-T.P. We thank Noldus, Wageningen, NL for the loan of an Erasmus Ladder for this study. We are indebted to Professor Chris De Zeeuw for discussion of our results. The views expressed are those of the author(s) and not necessarily those of the NHS, the NIHR or the Department of Health and Social Care.

ABSTRACT

We identify *Sox14* as an exclusive marker of inhibitory projection neurons in the lateral and interposed, but not medial, cerebellar nuclei. *Sox14*$^+$ neurons make up approximately 80% of *Gad1*$^+$ neurons in these nuclei and are indistinguishable by soma size from other inhibitory neurons. All *Sox14*$^+$ neurons of the lateral and interposed cerebellar nuclei are generated at around E10(.5) and extend long range, predominantly contralaterally projections to the inferior olive. A small *Sox14*$^+$ population in the adjacent, vestibular nucleus "Y" send an ipsilateral projection to the oculomotor nucleus. Cerebellar *Sox14*$^+$ and glutamatergic projection neurons assemble in non-overlapping populations at the nuclear transition zone and their integration into a coherent nucleus depends on *Sox14* function. Targeted ablation of *Sox14*$^+$ cells by conditional viral expression of diphtheria toxin, leads to significantly impaired motor learning. Contrary to expectations, associative learning is unaffected by unilateral *Sox14*$^+$ neuron elimination in the interposed and lateral nuclei.

SIGNIFICANCE STATEMENT (120 words maximum)

The cerebellar nuclei are central to cerebellar function, yet how they modulate and process cerebellar inputs and outputs is still largely unknown. Our study gives a direct insight into how nucleo-olivary projection neurons are generated, their projections and function in an intact behaving mouse. These neurons play a critical conceptual role in all models of cerebellar function and this study represents the first specific analysis of their molecular identity and function and offers a powerful model for future investigation of cerebellar function in motor control and learning.

INTRODUCTION

The cerebellum is characterised by a remarkably uniform neural structure that executes a repertoire of adaptive neural functions. Its ability to modulate output in a flexible and predictive manner relies on its position within a series of nested, re-entrant loops converging on the modulation of cerebellar nuclei output by inhibitory Purkinje cells. One key loop involves the inferior olive whose climbing fibre output can profoundly influence the activity of Purkinje cells and hence the activity of excitatory cerebellar nuclear efferents. In turn, the cerebellar output nuclei have both excitatory and inhibitory efferents and it is the descending, long-range inhibitory axons that modulate the output of inferior olive. This cerebello-nuclear-olivo circuit comprises parallel, loops passing via the lateral, interposed and medial nuclei, which are then further subdivided into discrete functional modules (Cerminara and Apps, 2011).

The nucleo-olivary pathway has been implicated in altering climbing fibre activity (Sears and Steinmetz, 1991; Hesslow and Ivarsson, 1996; Lang et al., 1996; Bengtsson et al., 2004; Lefler et al., 2014; Najac and Raman, 2015b), at least partly through modulating the gap junction connectivity within inferior olive sub-populations (Kistler et al., 2002; Van Der Giessen et al., 2008). This has been proposed to modulate both synchronous clustering of activity in the inferior olive, thought to be integral for motor timing (Lang et al., 1996; Leznik et al., 2002; Best and Regehr, 2009; Llinás, 2011, 2013), and a more selective weakening of specific olivary outputs during motor learning (Schweighofer et al., 2013) or associative learning tasks (Medina et al., 2002; De Zeeuw et al., 2003; Bengtsson et al., 2007). In either case, the role of nucleo-olivary input is to weaken olivary coupling by promoting shunting via gap junctions. However, no experimental study has managed to selectively disrupt the nucleo-olivary pathway *in vivo*.

Identifying the molecular identity of the long-range nucleo-olivary neurons is an important goal in understanding cerebellar function. Development offers a window into unique identifiers of neuronal populations. In the cerebellum, neuronal diversity is the product of exquisite temporal patterning

within a GABAergic, ventricular progenitor pool (Kim et al., 2008) and the glutamatergic rhombic lip pool, which borders the roof plate of the fourth ventricle (Gilthorpe et al., 2002; Machold and Fishell, 2005). These populations express distinct bHLH transcription factors, Ptf1a and Atoh1, respectively (Hoshino et al., 2005; Machold and Fishell, 2005; Wang et al., 2005) and give rise to the full complement of cerebellar neurons.

At the rhombic lip, glutamatergic projection neurons of each cerebellar nucleus are generated in discrete temporal cohorts at the rhombic lip (Green and Wingate, 2014), characterised by distinct markers (Wang et al., 2005; Fink et al., 2006). Neurons migrate tangentially to an intermediate assembly point known as the nuclear transitory zone (NTZ) (Altman and Bayer, 1985) and from there to the white matter. By contrast, little is known of the specification, migration or ultimate molecular identity of the Ptf1a-derived inhibitory projection neurons relative to other Ptf1a- derived cerebellar cell types (Hoshino et al., 2005; Kim et al., 2008; Zordan et al., 2008) or how integration of inhibitory and excitatory neurons within the nuclei is achieved. Molecular characterisation of inhibitory projection neurons thus offers the promise of insights into circuit assembly in addition to a precise functional analysis of how the inferior olive is regulated by the cerebellum.

We chose to address these questions surrounding neuron identity by investigating *Sox14,* an SRY-related gene, expressed in a range of inhibitory neurons in the CNS (Hargrave et al., 2000; McClellan et al., 2006; Delogu et al., 2012). Recent studies have shown that *Sox14* is required for tangential migration of GABAergic precursors in the thalamus and midbrain (Delogu et al., 2012; Jager et al., 2016). We found *Sox14* reporter expression in the lateral and interposed, but not the medial, cerebellar nuclei from E12.5 to P0. Axonal tracing techniques reveal that cerebellar *Sox14*-expressing cells comprise exclusively nucleo-olivary neurons, generated within the same temporal window as their glutamatergic long-range projecting counterparts. Unilateral ablation of *Sox14* neurons results in motor deficits and impaired motor learning, but not in impairment to associative learning.

METHODS

ANIMALS HUSBANDRY AND BIRTH-DATING EXPERIMENTS

The *Sox14*$^{Gfp/+}$ (Delogu et al., 2012) and *Sox14*$^{Cre/+}$ (Jager et al., 2016) mouse lines were maintained in the C57BL/6 background in the animal facilities of King's College London. All mice were housed in Techniplast cages (32cm x 16cm x 14cm) with sawdust (Litaspen premium, Datesand Ltd, Manchester, UK) and basic cage enrichment, consisting of sizzlenest (Datesand Ltd, Manchester, UK) and a cardboard shelter (LBS Biotech, Horley, UK). All mice had ad libitum access to water and food (Rat and Mouse No. 3 Diet (RM3) for breeders and No. 1 (RM1) for test mice; Special Diet Services, Essex, UK). The housing room was maintained at constant room temperature (~21 °C) and humidity (~45%) and kept under a regular light/dark schedule with lights on from 08:00 to 20:00 hours (light = 270 lux). All experimental procedures described have received internal approval by the King's College London Ethical Committee and are covered by a UK Home Office License 70/9042. For birth dating cells, BrdU (Sigma, B5002) was administered intraperitoneally (in saline: 0.2 mg g−1) into a subset of pregnant mice at 09:00 between E10.5 and 18.5, estimated from the occurrence of a vaginal plug (morning of the day the plug was detected was designated E0.5). Embryos from uninjected dams were harvested for morphological analysis at E11.5 and E12.5. A proportion of neonatal animals were euthanised at P0 (decapitation). Some brains were set aside from primary cell culture while the others were immersion fixed in 4% paraformaldehyde in saline. Pups from BrdU injected dams were sacrificed at P7. The remaining litters were selected for steroataxic injection at P14 for tract tracing and behavioural experiments or sacrificed at P21 for morphological analysis. At these later stages, mice were euthanized with 0.6 ml/kg of pentobarbital sodium 20% w/v i.p. (Pentoject) administered intraperitoneally and then perfused with 4% paraformaldehyde in saline. Only adult (above 8 weeks) male mice were used for behavioural tests.

PRIMARY CELL CULTURE

The entire cerebellum at P0, comprising cortex and nuclei was dissected out immediately in ice cold sterile PBS and transferred into ice-cold HEPES buffer and dissociated both mechanically and enzymatically (papain, EDTA, DNAse, Neurobasal, L-cysteine). Neurobasal medium. A final dissociation step by trituration with a polished glass pipette in Neurobasal medium (Neurobasal, B27, Glutamax, antibiotic-mycotic solution: GIBCO) resulted in a cell suspension that was plated overnight onto poly-D-Lysine (Myat et al., 1996) coated coverslips at a density of $2x10^5$ cells per well and incubated overnight at 37°C.

STEREOTAXIC BRAIN INJECTIONS

P14 animals of both sexes were used for tract tracing experiments. Only males were used for targeted ablation experiments and behavioural tests. Animals were anaesthetised using isoflurane and injections were made stereotaxically into the cerebellar nuclei, inferior olive or oculomotor nucleus or combinations of these sites. For anterograde tracing of *Sox14* expressing cells, 0.2-0.8 µl of *Cre*-dependent adenoassociated virus (pAAV-EF1a-DIO-mGFP (serotype 2/1, 5.9 $x10^{13}$ vg/ml) or pAAV-EF1a-DIO-tdTom (serotype 2/1, 1.6 $x10^9$ vg/ml), gifted from Dr Botond Roska) was injected in the brains of $Sox14^{Cre/+}$ mice at coordinates relative to lambda: x, y, z = ±2.00, −1.60, −3.85 mm to target the cerebellar nuclei; ±0.10, +0.10, −2.50 mm to target the oculomotor nucleus; ±0.10, −1.90, −5.00 mm to target the inferior olive. For retrograde tracing, target nuclei in the brains of $Sox14^{Gfp/+}$ mice were injected with 100 nl of fluorescent latex "RetroBead" microsphere solution (Lumafluor). Targeted ablation of $Sox14^+$ cells in $Sox14^{Cre/+}$ mice was achieved by targeted injections of AAV-mCherry-flex-dtA (Addgene plasmid # 58536) (serotype 2/1, 6.0 $x10^{12}$ vg/ml) for the experimental animals, while sham injections were carried out using AAV-EF1a-DIO-tdTom in $Sox14^{Cre/+}$ mice, or AAV-mCherry-flex-dtA in $Sox14^{+/+}$ mice. AAV-mCherry-flex-dtA encodes a subunit of the diphtheria toxin in the *Cre*-expressing cells while also promoting the non-*Cre*-dependent production of a mCherry red fluorescent protein in all cells infected by the virus, thus allowing postmortem analysis of the site of injection.

BEHAVIOURAL TESTS

Motor learning and coordination were assessed using a Rota-Rod 47600 testing device (Ugo Basile, Milan, Italy). Mice were tested over 3 days, with 24 hr between the sessions. On each day, mice underwent 3 trials, at1 hr intervals. On each trial the rod was set to accelerate from 2rpm to 40rpm over 300s. Latency to fall was measured as the time from the start of the acceleration of the rod to the point the mouse fell onto the sensor below the rod. If the mouse clung to the rod to rotate around with it more than 3 consecutive rotations instead of falling, this was also deemed the end of the trial, since this implies an inability to maintain locomotion at that speed.

Locomotive performance and associative motor learning were assessed on an Erasmus Ladder v1.1 (Noldus, Netherlands)(Vinueza Veloz et al., 2015). This consists of a horizontal ladder of 2 x 37 touch sensitive rungs (4 gram threshold) for the left and right side, with alternate rungs in a descended position to create an alternating stepping pattern with 30 mm gaps. Motor performance is assessed by the number of missteps (lowered rungs that are stepped on). Each mouse was tested over 10 days, with 4 days training to cross the ladder without obstacles, followed by 2 days of rest, and another 4 days of an associative motor learning test. Each day, 42 trials were performed consecutively for each mouse.

For the associative motor learning paradigm, a third set of rungs whose default position is lowered, were employed as obstacles. Based on the prediction of the position of the mouse and the speed of walking, an obstacle rung can be raised by a high-speed pneumatic slide. This perturbation acts as an unconditioned stimulus (US). A 90 dB, 2 kHz tone lasting by default 250 ms, was used as a conditioned stimulus (CS) at a fixed interval prior to the unconditional stimulus. The ladder records the change in step time for each mouse before and after perturbation. The difference between pre- and post-perturbation steptime (Δ steptime) before and after conditioning are a readout of motor learning (Van Der Giessen et al., 2008).

IN SITU HYBRIDISATION AND IMMUNOLABELLING

Primary cell cultures, and floating cryosections at 60 µm were prepared for immunostaining, while 20 µm cryosections on slides were prepared for *in situ* hybridization. *In situ* hybridisation was carried out using standard protocols (Myat et al., 1996) using the following riboprobes, *Gad1 (IMAGE: 5358787)*, *Gad2* (IMAGE: 4482097), *PValb* (IMAGE: 4925213), *Calb2* (IMAGE: 4527074). Immunostaining was carried out using standard protocols with antibodies against: GFP (chicken, Abcam, 1:10000), dsRed (rabbit, Clontech, 1:200), GABA (rabbit, Sigma-Aldrich, 1:2000), PValb (rabbit, Abcam, 1:400), Calb1 (mouse, Abcam, 1:400), Calb2 (rabbit, Abcam, 1:200), MAP2 (mouse, Sigma-Aldrich, 1:1000), Lhx1/5 (mouse, DHB, 1:20), Pax6, (mouse, DHB, 1:100), BrdU (rat, Bio-Rad, 1:200), vGAT (rabbit, Synaptic Systems, 1:600) and appropriate fluorescent Goat Alexa-568 anti-rat and Alexa-488 anti-chicken secondary antibodies (Invitrogen). For animals from BrdU injected dams, cryosections were preincubated in 1 M HCl in H_2O at 45 °C for 30 min.

IMAGING AND ANALYSIS

Labelled brains were imaged on a compound epifluorescence microscope (ZEISS Axio Imager 2712) equipped with a Zeiss ApoTome. a spinning disk confocal microscope (Nikon Eclipse Ti Inverted) or a laser scanning confocal microscope (Olympus Fluoview AX70, Eclipse Ni-E Upright, Nikon).

EXPERIMENTAL DESIGN AND STATISTICAL ANALYSIS

In order to control for the behavioural results, only male mice were used for the ablation experiment. 20 $Sox14^{Cre/+}$ mice and 20 $Sox14^{+/+}$ mice were used. Either *Cre*-dependent AAV-mCherry-flex-dtA or AAV-DIO-tdTom (control) were injected bilaterally into the cerebellar nuclei of both genotypes, thus creating 1 experimental group and 3 control groups. To ensure statistical power is maximized, while minimising the number of animals used, more mice were injected with

AAV-mCherry-flex-dtA (*Sox14*$^{Cre/+}$: n= 16; *Sox14*$^{+/+}$: n= 12), than AAV-DIO-tdTom (*Sox14*$^{Cre/+}$: n= 4; *Sox14*$^{+/+}$: n= 8).

In order to gauge the size of the *Sox14*$^{+}$ cells relative to the cell types described in other (Chan-Palay, 1977; Legendre and Courville, 1987; Aizenman et al., 2003; Uusisaari et al., 2007; Bagnall et al., 2009; Uusisaari and Knopfel, 2012; Najac and Raman, 2015a) literature , a sample of cells (210 cells across n= 5 brains) were measured for soma size as defined by the cross-sectional area of the cell body on the image plane, and the mean diameter. To measure the approximate size of cell soma, the selection tools were used to draw around the cell soma. The "Measure" tool in ImageJ was set to measure the area of the selection (taken as the soma cross-sectional area) as well as the "Fit ellipse" measurement, which reports the major and minor axis of the best fitting ellipse as the minimum and maximum diameters of the selected area. The soma diameter was calculated by taking the average of the maximum and minimum diameter of each soma. For counting the proportion of of co-expression of immunoreactivity, the "cell counter" plugin was used to manually label each cell in an image.

Statistics and charts were created using Prism 7 software (GraphPad). To analyse the behavioural data, all the control animals were pooled into one group "Sham". For normally distributed results, Student's t-test and two-way ANOVAs were conducted with Bonferroni's multiple comparisons test or Corrected method of Benjamini and Yekutieli to control the False Discovery Rate. Charts present the mean ± standard error of the mean. For non-parametric data, the Mann-Whitney U test was used to test if the independent sham and experimental groups have the same distribution and the charts present the median with 95% confidence limit.

Automated counts of *Gad1*-positive cells were used in cell ablation experiments using defined regions of interest (ROI) were and the "Find Maxima…" function in ImageJ, using a macro to automate the count. This produced a tabulation of the number of cells detected in each ROI, while a flattened image with each detected cell was saved to check for errors in the counting. If a particular

image had a severe miscount (over or under estimate of the number of cells) due to inconsistency in staining, the detection threshold was adjusted accordingly.

RESULTS

SOX14 IDENTIFIES A CEREBELLAR NUCLEUS CELL TYPE EXCLUSIVE TO THE LATERAL AND INTERPOSITUS NUCLEI

We found expression *Sox14* in the cerebellum of *Sox14*$^{Gfp/+}$ mice from E12.5 to P28 (data not shown). A series of coronal sections at P14 from rostral to caudal shows *Sox14*$^{+}$ cells are distributed irregularly in the lateral nucleus, but with a higher density ventromedially (Fig.1A). Midway through the cerebellum (Fig.1B&C) distribution can be directly compared in the lateral, interposed and medial cerebellar nuclei, with the superior vestibular nucleus and vestibulocerebellar nucleus that lie directly below the posterior interposed nucleus. *Sox14*$^{+}$ cells are sparsest in the dorsal regions of the nuclei, particularly in the dorsolateral and anterior interposed nuclei. In contrast, *Sox14*$^{+}$ cells are present at a high density in the parvicellular domain on the ventral border of the lateral nucleus. *Sox14*–positive cells are also found in superior vestibular and vestibulocerebellar nuclei. The medial nucleus does not contain *Sox14*$^{+}$ cells, with the exception of a scattering of cells in the rostroventral medial nucleus (Fig.1C, boxed region and inset). In more caudal sections the medial nucleus is devoid of *Sox14*$^{+}$ cells (Fig1.D).

SOX14-POSITIVE CELLS COMPRISE AT LEAST 2 MOLECULARLY DISTINCT POPULATIONS OF SMALL, GABAERGIC NEURONS.

We used immunohistochemistry and *in situ* hybridisation to examine the molecular phenotype of *Sox14*$^{+}$ cells in the *Sox14*$^{Gfp/+}$ cerebellum at P0 and P21. At P21, GFP and GABA colocalise in the cytoplasm of *Sox14*$^{+}$ neurons (Fig.2A, white arrowheads). Because the of density of GABA-positive axon terminals within the nucleus neuropil, colocalisation of GABA with GFP was confirmed by immunocytochemistry on primary cultures of dissociated P0 *Sox14*$^{Gfp/+}$ cerebellar tissue (Fig.2B). In all instances, GFP co-localised with GABA and the pan-neuronal marker MAP2 (n=21). Detection of *Gad1* (Fig.2C) and *Gad2* (Fig.2D) mRNAs by *in situ* hybridization and GFP immunohistochemistry on *Sox14*$^{Gfp/+}$ at P21, revealed that *Sox14*$^{+}$ neurons are a subset of the entire GABAergic population within the cerebellar nuclei. In the medial nucleus, all *Gad1*–positive cells

are GFP-negative (data not shown) consistent with the observation that *Sox14*$^{+}$ neurons are absent from this nucleus. The *Sox14*$^{-}$ fraction within the other cerebellar nuclei accounts for 27% of *Gad1*–positive cells and 20% of *Gad2*–positive cells (n=5 brains).

Sox14^{+} neurons are negative for PValb (Fig.2E), Calb1 (Fig.2F,) and Calb2 (Fig.2G). *In situ* hybridization revealed that *PValb*$^{+}$ neurons are larger in size (Fig.2H), and contrast the regional distribution of *Sox14*$^{+}$ neurons: GFP^{-}/PValb^{+} mostly lie in the dorsal lateral nucleus, posterior interposed and medial nuclei (Fig.2F), while the smaller GFP^{+}/PValb^{-} cells which are most populous in the ventromedial region of the lateral nucleus. *In situ* hybridisation for *Calb2* reveals two populations of *Sox14*$^{+}$ neurons within the lateral cerebellar nucleus; the *Calb2*$^{+}$/ GFP^{+} neurons reside in the ventromedial regions while the rest of the *Sox14*$^{+}$ neurons throughout the nuclei are *Calb2*$^{-}$ (Fig.2I). Other *Calb2*$^{+}$ cells are seen in the superior vestibular nuclei and vestibulocerebellar nuclei, as well as the cochlear nuclei more ventrally.

We used *in situ* hybridization data on brain slices (N=5 brains per probe) to map the average relative soma sizes of GFP^{+}/*Gad1*$^{+}$, GFP^{-}/*Gad1*$^{+}$ and GFP^{-}/*PValb*$^{+}$ cells in terms of mean cross sectional area and diameter. The mean soma cross-sectional areas are as follows: GFP^{+}/*Gad1*$^{+}$ 153.4 ± 5.8 μm^2; GFP^{-}/*Gad1*$^{+}$ 170.7 ± 8.5 μm^2; and GFP^{-}/*PValb*$^{+}$ 381.4 ± 10.4 μm^2 (mean±SEM). The mean soma diameters are as follows: GFP^{+}/*Gad1*$^{+}$ 14.1 ± 0.3 μm; GFP^{-}/*Gad1*$^{+}$ 15.1 ± 0.4 μm; and GFP^{-}/*PValb*$^{+}$ 22.3 ± 0.3 μm (mean±SEM). Figure 2J shows that while the mean soma diameters is larger for GFP^{-}/*Gad1*$^{+}$ cells compared to GFP^{+}/*Gad1*$^{+}$ cells, the two populations have overlapping diameter distributions that are not significantly different. This is more clearly seen in a scatter plot of diameters (Fig.2K) where the whole range of GFP^{-}/*Gad1*$^{+}$ cells measured falls within the large range of GFP^{+}/*Gad1*$^{+}$ cell diameters.

SOX14-POSITIVE NEURONS APPEAR TO BE EXCLUSIVELY PROJECTION NEURONS

To investigate the trajectory of *Sox14*$^{+}$ GABAergic nuclear axons, the lateral cerebellar nuclei of *Sox14*$^{Cre/+}$ heterozygous mice were unilaterally, stereotaxically targeted for injection with AAV-EF1a-DIO-mGFP tracer at P14 and collected for analysis at P28 (*n*=14) (Fig.3A). The majority of labelled axons of these cells project decussate at the superior cerebellar peduncle (Fig.3B: xscp), as the "horseshoe–shaped commissure of Wernekinck" and descend to terminate in the contralateral inferior olive (Fig.3C). Ipsilaterally, ascending axons also extend into the midbrain, terminating in the oculomotor nucleus (Fig.3D), while a small population of descending axons target the inferior olive.

To assess the respective contributions of contralateral and ipsilateral projections to inferior olive sub-nuclei, *Sox14*$^{Cre/+}$ brains were injected with AAV-EF1a-DIO-mGFP in the cerebellar nuclei of one hemisphere and with AAV-EF1a-DIO-tdTom at symmetrical coordinates on the other side of the brain. Fluorescently labelled axon terminals reveal a contralateral and a relatively sparse ipsilateral projection pattern (Fig.3E). The principal olive, ventrolateral protrusion and the cap of Kooy of the medial nucleus receive a bilateral, predominantly contralateral, input. Nucleo-olivary axons leave gaps where olivary cells reside, as confirmed by nuclear DAPI staining (Fig.3F). Axonal boutons cluster in acellular spaces suggesting that synapses are concentrated distant to the cell body.

To examine whether the projections to the oculomotor nucleus are also derived from cerebellar *Sox14*$^{+}$ neurons, green fluorescent latex microspheres (RetroBeads) were injected into the ipsilateral oculomotor nuclei (Fig.4A) and red RetroBeads into the contralateral inferior olive (Fig.4B) of *Sox14*$^{Gfp/+}$ mice (n=10). Retrogradely transported green RetroBeads from the oculomotor nucleus were not transported to the cerebellar nuclei, but rather, were found just lateral to the superior vestibular nucleus, directly ventral to the parvicellular lateral cerebellar nucleus. This region corresponds to Nucleus Y (or Group Y) and contains both *Sox14* positive and negative

cells that project to the oculomotor nucleus (Fig.4C). Both red and green RetroBeads label *Sox14*$^{+}$ neurons, but no neurons are co-labelled with both retrograde tracers (Fig.4C').

To determine whether *Sox14*$^{+}$ neurons make up the entire GABAergic efferent projection to the inferior olive, green RetroBeads were injected unilaterally into the inferior olive of *Sox14*$^{Gfp/+}$mice at P19 (Fig.4D) and their retrograde transport examined after 2 days at P21. Within the lateral and interposed nuclei, RetroBeads were detected exclusively in *Sox14*$^{+}$ neurons (Fig.4E). We conclude that *Sox14* expressing cells are the only cell type in the lateral and interposed cerebellar nuclei that project to the inferior olive. However, we cannot formally exclude the possibility that some Sox14 cells may be interneurons. The ipsilateral and contralateral cell bodies labelled by the same injection site have a similar distribution across the cerebellar nuclei, while the number of cells in which beads are detected are noticeably fewer in the ipsilateral nucleus (Fig.4F).

Figure 4G schematically summarises the projection patterns of *Sox14*$^{+}$ neurons in the cerebellar and vestibular nuclei (left) and their targeting of different sub-nuclei within the inferior olive (right), revealed by anterograde and retrograde tracing. Projections from *Sox14*$^{+}$ neurons in the lateral cerebellar nucleus mainly target the principle olive and the dorsomedial cell group; the interposed nuclei project to the medial olivary nucleus and the dorsal olivary nucleus; and the vestibular nuclei target the cap of Kooy of the medial nucleus and the ventrolateral protrusion.

CEREBELLAR SOX14-POSITIVE NEURONS ARE GENERATED BETWEEN E10.5 AND E11.5 AND ACCUMULATE AT THE NTZ

In the developing rhombencepahlon, GFP in the cerebellum of *Sox14*$^{Gfp/+}$ is first seen at E10.5 and limited, until E11.5, to a ventral column of cells spanning the length of the hindbrain (Fig.5A,B). GFP expression is first seen in the cerebellar anlage at E12.5 in a band of cells in dorsal rhombomere 1, distal to the rhombic lip (Fig.5C). The precise birth date of *Sox14*$^{+}$ neurons was determined by injecting BrdU into pregnant dams at successive stages from E10.5-E18.5. The brains of the mice pups were collected and analyzed at P7. GFP^{-}labelled neurons incorporated BrdU

for injections administered at E10.5 (Fig.5D) and E11.5 (not shown). For injections made E12.5 or later, no BrdU staining was seen in GFP^-labelled cells (Fig.5E). Within the cerebellar cortex, BrdU was detected in Purkinje cells for injections made at E11.5, E12.5 and E13.5, showing the nucleo-olivary neurons are born prior to GABAergic Purkinje cells and interneurons (not shown). $Sox14^-$ /$BrdU^+$ cells are seen in the cerebellar nuclei throughout all the injections, showing that the other nuclear cell types are also generated during this time window.

Sox14$^{Gfp/+}$ E12.5 sagittal slices were stained using antibodies against Lhx1/5 and Pax6, which are expressed by well-characterised neuronal cell types of the developing cerebellum. *Lhx1/5* is expressed in Purkinje cells that are derived from the ventricular zone (Morales and Hatten, 2006), while *Pax6* expression defines the glutamatergic cell populations that migrate from the rhombic lip, including nucleus neurons that accumulate at the NTZ. At E12.5, GFP-expressing cells also label for Lhx1/5 (Fig.5F) and form a distinct pool of neurons superficial to the majority of *Lhx1/5*$^+$ cells, which represent Purkinje cells that are radially migrating from the ventricular zone. At high magnification, it is clear that the processes of GFP^+/Lhx1/5^+ neurons are aligned tangentially rather than radially. Staining for Pax6 (Fig.5G) reveals that GFP^+ cells lie adjacent and inferior to the glutamatergic nuclear neurons of the NTZ, which are known to express *Pax6* and tangentially migrating from the rhombic lip. Thus, *Sox14*$^+$ cells do not co-express *Pax6* and are distinct from the rhombic lip derivatives. The distribution of *Sox14* cells with respect to the NTZ is shown schematically for an E12.5 brain in Figure 5H.

Although the precise time course of the migration of GABAergic (*Sox14*$^+$) and glutamatergic (*Pax6*$^+$) nuclear populations to form the cerebellar nuclei could not be determined, an analysis of the *Sox14*$^{Gfp/Gfp}$ (knock-out) mouse at P0 indicates that migration of *Sox14*$^+$ neurons stalls before reaching their final location in the absence of a functional *Sox14* allele. At P0, the presumptive boundaries cerebellar nuclei can already be traced in the cerebellum of a *Sox14*$^{Gfp/+}$ brain (Fig.5I, I'). Conversely, in P0 *Sox14*$^{Gfp/Gfp}$ mice, GFP-expressing cells accumulate at the margins of

interposed and lateral nuclei and are excluded from their central regions (Fig.5J, asterisk). In adult (P42) mice, the normal high density of vGAT labelling in the IO (Fig.5K) is decreased in mutant mice (Fig.5L,M), consistent with a loss of GABAergic input from Sox14-positive projection neurons.

TARGETED ABLATION OF SOX14 CELLS LEADS TO MOTOR AND MOTOR LEARNING DEFICITS

Sox14^{+} neuron specific cell ablation in the cerebellar nuclei was achieved by conditional expression of diphtheria toxin A. Male mice were injected at P14 with *Cre*-dependent AAV-mCherry-flex-dtA (*Sox14*$^{Cre/+}$: n= 16; *Sox14*$^{+/+}$: n= 12), or control marker virus AAV-DIO-tdTom (*Sox14*$^{Cre/+}$: n= 4; *Sox14*$^{+/+}$: n= 8). Each animal was subjected to a suite of behavioural tests from 8 weeks old (6 weeks post-injection) and the post-mortem brains were analysed to assess the extent of *Sox14*$^{+}$ neuron ablation in each animal. Targeting was assessed by mCherry fluorescence and revealed that the anterior interposed nucleus on either side was the most frequently targeted nucleus (n=26/32), while fewer injections hit the medial (n=13/32) and posterior interposed nuclei (n=14/32). Off-target injections to the vestibular nuclei (n=17/32) were a potentially confounding factor in motor testing. A control density map of *Gad1*$^{+}$ neurons was constructed from cerebellar nuclei of sham injected littermates (n=24) and used to estimate the reduction in *Sox14*$^{+}$ neurons upon cre-dependent dtA expression (Fig.6A). As expected from mCherry distribution, when cell survival is assessed in the entire experimental population (n=16), average loss is differentially highest in the anterior interposed nucleus (Fig.6B). Mice with more than 70% loss of *Gad1*$^{+}$ cells (n=6) were retrospectively identified as a distinct group (Fig.6C).

Motor learning was measured as latency to fall in an accelerating Rotarod task. Fig.6D shows the assessment of all experimental animals against the sham injected group while Fig.6E only shows the motor data for the selected experimental sub-group. While the experimentally ablated animals display an acquisition curve over time, similar to the sham controls, and start from similar levels of latency on day 1, the latency to fall in the experimental group was significantly shorter at day 2 and

at day 3 compared to sham scores on those days (p=0.0324 and p=0.0374, respectively). Overall, the latency to fall was significantly shorter than in animals injected with control virus (two-way ANOVA: main effect of ablation, F (1,120) = 4.479, P = 0.0064). These results show that ablation of Sox14-positive cells reduces the ability to acquire the motor skills needed to stay on the accelerating rod.

To test basic motor coordination, the number of missteps in a smaller group of sham-injected littermates (n=10) and experimentally ablated mice (n=10) were assessed on introduction to the regularly spaced, pressure-sensitive rungs (30 mm gaps) on an Erasmus ladder (42 consecutive trials). Experimental animals with ablated nuclei exhibited a significantly higher median percentage of missteps on day 1 (Fig.6F, p = 0.0433, Fig.6G). This difference is ameliorated over the subsequent days of trials on the ladder and there is no significant difference median percentage of missteps after training by day 4 (data not shown). Over these training days, experimental animals and sham-injected animals showed a similar overall average step time (sham: 339 ± 23.5 ms; experimental animals 358 ± 29 ms) but significant differences in stepping pattern (Fig.6H-J). While both groups showed increasing familiarity with the ladder as reflected in a significant increase in long steps (Fig,6H: p< 0.0001) and reduction in back-steps (Fig,6I: p< 0.0001) over trial days, the experimental group jumped significantly fewer times than the sham group (Fig,6J: two-way ANOVA, p= 0.0033, F (1, 80) = 9.20). This suggests a reduced competence in motor function, matching the initially higher misstep rate in this group (Fig,6F).

Following the 4 days of training on the ladder, the mice were then tested over subsequent days 5-8 with a conditioned learning paradigm. The instantaneous introduction of an obstacle rung, which disturbs the stepping pattern (Fig.6G), was used as an unconditioned stimulus. A 90 dB, 2 kHz tone lasting 250 ms was used as a conditional stimulus 250 ms prior to the introduction of the obstacle. The length of time needed to overcome the obstacle (post-perturbation step-time) was measured. On trial days, each mouse was given either unperturbed trials, paired trials or a conditioned stimulus

only trials, or unconditioned stimulus only trials as summarized in Figure 6K. Post-perturbation step-times are similar to the average step-times on days 1-4. When the obstacle is first introduced on day 5, mice in both experimental and sham groups show a significant increase in post-perturbation step-time. This reduces over the course of 4 days of successive trials for both paired and unconditioned stimulus only trials. Therefore, in contrast to Rotarod experiments, both groups of animals showed an equivalent improvement in ability (reduced post-perturbation step-time) to bypass an instantaneously raised rung. When the obstacle is preceded by an auditory cue, mice in both groups show a significantly more rapid habituation to the obstacle and post-perturbation step-times are shorter, indicating an ability to predict the imminent obstacle. Learning in both experimental and sham groups was not significantly different for any of the trial types. Therefore, both groups show an equal associative learning through the introduction of a conditional cue prior to the introduction of an obstacle.

DISCUSSION

In this study we show that *Sox14* defines at least two molecularly distinct populations of GABAergic projection neurons in the lateral and interposed nucleus that project both contralaterally and ipsilaterally to the inferior olive. A small population of *Sox14*$^{+}$ neurons in Nucleus Y of the vestibular nucleus projects to the ipsilateral oculomotor nucleus. Ablation of the interposed nucleus population leads to defects in motor function and motor learning, but not to any deficit in associative motor learning.

SOX14 IS A GENETIC MARKER FOR NUCLEO-OLIVARY NEURONS IN THE LATERAL AND INTERPOSED NUCLEI

Within the lateral and interposed nucleus, our results show that *Sox14* is expressed exclusively in GABAergic projection neurons that target the inferior olive. Our axonal mapping data concurs with previous tracer studies that have shown both the location of projection neurons within nuclei and the orderly topographic projection of each nucleus to the different olivary sub-nuclei (Tolbert et al., 1976; Brown et al., 1977; Buisseret-Delmas and Batini, 1978; Legendre and Courville, 1987; Giaquinta et al., 1999). We also identify *Sox14* neurons in nucleus Y that account for the previously characterized ipsilateral projection from this region to the oculomotor nucleus (Graybiel and Hartwieg, 1974; Steiger and Buttner-Ennever, 1979; Stanton, 1980; Yamamoto et al., 1986). Due to the modular nature of the nucleo-olivary circuit, it is possible to speculate that *Sox14* neurons would broadly have a role in higher cognition, motor planning (lateral nucleus), visuomotor control (ventromedial lateral nucleus), and associative learning (interposed nucleus). The nucleus Y projection is involved in the regulation of the vertical vestibulo-ocular reflex (Chubb and Fuchs, 1982; Highstein et al., 1997). The significance of a sub-population of Calretinin-positive Sox14-positive projection neurons is unclear. In the lateral nucleus, *Sox14* expression in the ventromedial, parvicellular lateral nucleus maps to the location of inferior olive projection neurons identified in previous mapping experiments and hence to the bulk of the Calretinin population. This cluster is not associated with the laterality of projection: by contrast, ipsilaterally and contralaterally projecting

neurons are evenly distributed across the nuclei. *Sox14* neurons account for the majority, but not all, of the GABAergic neurons in the lateral and interposed nuclei. The Sox14-negative inhibitory fraction comprises both local interneurons but also projection neurons that send inhibitory connections to the cerebellar cortex (Uusisaari and Knöpfel, 2011; Houck and Person, 2014). This difference is visualised in the Allen Mouse Brain Connectivity Atlas Projection data using the Slc32a1-IRES-Cre mouse, where Slc32a1 is expressed in all inhibitory cell types; Cre-dependent AAV injections reveal additional projections from the cerebellar nuclei to the cerebellar cortex that are not seen using the Sox14-Cre mouse. Cell body size distribution does not distinguish these different groups. All are relatively small compared to the Parvalbumin-positive (presumably glutamatergic projection) neurons that have a roughly complementary distribution within the nuclei.

OLIVARY PROJECTION NEURONS ARE A DISTINCT EARLY BORN COHORT OF GABAERGIC DERIVATIVES

Our data reveals a striking absence of *Sox14* neurons in the medial nucleus suggesting that its descending inhibitory projection has distinct embryonic origins. The medial nucleus displays a unique GABAergic marker, *Zac1* (Chung et al., 2011) and the descending olivary projection from the medial nucleus projects along its own distinct tract (Dom et al., 1973; Martin et al., 1976; Legendre and Courville, 1987). This may correspond to its presumed phylogentically more ancient origin (Green and Wingate, 2014) linked to reflex motor functions such as the vestibulo-ocular reflexes, optokinetic control and saccades (Ito, 2013). Ito further argues the medial olivo-cerebellar module is distinct in its capacity to drive motor patterns in contrast to the more modulatory function of other nuclei. The medial is also the only nucleus to contain large glycinergic neurons, which project to vestibular and reticular hindbrain targets (Bagnall et al., 2009; Chung et al., 2009).

Developmentally, both *Lhx1/5*-positive *Sox14* neurons and *Zac1*-positive cells (Chung et al., 2011) lie adjacent to the NTZ where rhombic lip derived glutamatergic nuclear cells assemble at E12-13. All GABAergic cerebellar neurons are derived from precursors that express *Ptf1a* (Hoshino et al., 2005). The birth date of *Sox14* cerebellar neurons (E10.5) also corresponds to a transient early

expression of *Ascl1* in the ventricular zone (Kim et al., 2008) and *Neurog2* (Zordan et al., 2008), suggesting that, as in the diencephalon, *Sox14* neurons transiently express *Ascl1* (Delogu et al., 2012). GABAergic nuclear neurons produced during a later wave of *Ascl1* expression in *Ptf1a* precursors (E13-16) likely correspond to local interneurons that are also characterized by *Neurog1* (Lundell et al., 2009) and *Pax2* expression (Maricich and Herrup, 1999). Our results suggest that the early wave of GABAergic cell production in *Ascl1*/*Ptf1a* progenitors exclusively generates projection neurons and is remarkably synchronized to the production of glutamatergic neurons from the rhombic lip, as well as to the production of olivary cells which send up climbing fibres (Hoshino, 2012; Pierce, 1973). Like rhombic lip derivatives, *Sox14* neurons are tangentially orientated at the NTZ suggesting some capacity for non-radial migration. *Sox14* itself appears to be required for the successful integration of populations into a nucleus, however, we cannot determine whether Sox14 is required for an olivary axon projection, particularly since the medial nucleus GABAergic nuclear projection is Sox14-independent. When *Sox14* is deleted, we find that cells are unable to migrate into their normal location, reminiscent of its role in facilitating migration in the formation of an integrated excitatory and inhibitory dorsal thalamus (Delogu et al., 2012; Jager et al., 2016).

THE ROLE OF THE NUCLEO-OLIVARY PROJECTION IN MOTOR FUNCTION AND LEARNING

We used a bilateral, conditional viral-mediated ablation protocol to test the function of *Sox14* neurons and revealed a significant deficit in motor coordination (missteps on walking a ladder), which improved with experience, and impaired learning on a balance test (Rotarod). In contrast to expectations (Medina et al., 2002), there was no impairment to associative learning where both experimental and control groups showed a positive response to priming an obstacle task with a conditioned auditory stimulus.

Viral injections produce varying degrees of cell loss within the cerebellar nuclei and it is possible that a more complete ablation might have led to stronger learning defects. Similarly, for associative

learning, a range of approaches (including eye-blink conditioning and investigations into extinction, reacquisition and blocking of conditioned responses) might show functions of the nucleo-olivary feedback that were not tested in the present study. Nevertheless, our study represents the first selective experimental ablation of nucleo-olivary projection neurons and implications of our observations are that either cerebello-olivary inputs are not involved in non-associative learning rather than associative learning, or that they are partially redundant to other GABAergic inputs to the olive (Geborek et al., 2012). There is strong evidence that activity in descending inhibitory axons decreases the extent of coupling between inferior olivary neurons (Lefler et al., 2014) and, by implication, the synchronous activity of Purkinje cells, which they in turn excite. Our results are consistent with coupling playing a role in fine tuning of motor learning (Schweighofer et al., 2013). We find that learning is not abolished but significantly less efficient following ablation of *Sox14* neurons.

Our results contrast with the consequences of constitutively reduced electrotonic coupling in the inferior olive in the *Cx36* knockout mouse (Van Der Giessen et al., 2008). In the latter model, while a similar impairment of basic motor function is revealed on the Erasmus ladder test, there is non-accompanying significant deficit in associative learning. A parsimonious explanation is that conditioning in this task relies on bilateral brain function and that intact unilateral pathways from incomplete ablation are sufficient to mask any deficit. Similarly sprouting of axons to the damaged nuclei from the contralateral, intact olive (Sugihara et al., 2003; Dixon et al., 2005) or regulation within olivary neurons themselves (Long et al., 2002; De Zeeuw et al., 2003) may provide a developmental compensation for aberrant function. More intriguing, our results may indicate that the nucleo-olivary input is not the sole regulator of gap junction coupling in the inferior olive pointing to a role for other pathways in modulating cerebello-olivary feedback (Geborek et al., 2012).

CONCLUSIONS

In summary we show, *Sox14* exclusively identifies GABAergic nucleo-olivary projection neurons of the interposed and lateral nuclei. The medial cerebellar nucleus has an anatomically and genetically distinct olivary projection. *Sox14*-positive cells appear are the earliest born cohort of GABAergic neurons, generated contemporaneously with glutamatergic nuclear neurons at the rhombic lip, which co-assemble at the NTZ and then integrate as a series of nuclei in a *Sox14*-dependent mechanism. Finally, targeted partial ablation of $Sox14^{+}$ cells in the cerebellar nuclei leads to significant deficits in motor learning, but not to an impaired associative learning.

REFERENCES

Aizenman CD, Huang EJ, Linden DJ (2003) Morphological correlates of intrinsic electrical excitability in neurons of the deep cerebellar nuclei. Journal of neurophysiology 89:1738-1747.

Altman J, Bayer SA (1985) Embryonic development of the rat cerebellum. II. Translocation and regional distribution of the deep neurons. J Comp Neurol 231:27-41.

Bagnall MW, Zingg B, Sakatos A, Moghadam SH, Zeilhofer HU, du Lac S (2009) Glycinergic projection neurons of the cerebellum. The Journal of Neuroscience 29:10104-10110.

Bengtsson F, Svensson P, Hesslow G (2004) Feedback control of Purkinje cell activity by the cerebello-olivary pathway. Eur J Neurosci 20:2999-3005.

Bengtsson F, Jirenhed DA, Svensson P, Hesslow G (2007) Extinction of conditioned blink responses by cerebello-olivary pathway stimulation. Neuroreport 18:1479-1482.

Best AR, Regehr WG (2009) Inhibitory regulation of electrically coupled neurons in the inferior olive is mediated by asynchronous release of GABA. Neuron 62:555-565.

Brown JT, Chan-Palay V, Palay SL (1977) A study of afferent input to the inferior olivary complex in the rat by retrograde axonal transport of horseradish peroxidase. J Comp Neurol 176:1-22.

Buisseret-Delmas C, Batini C (1978) Topology of the pathways to the inferior olive as ? study in cat. Neurosci Lett 10:207-214.

Cerminara NL, Apps R (2011) Behavioural significance of cerebellar modules. The Cerebellum 10:484-494.

Chan-Palay V (1977) Cerebellar dentate nucleus : organization, cytology and transmitters. Berlin: Springer.

Chubb MC, Fuchs AF (1982) Contribution of y group of vestibular nuclei and dentate nucleus of cerebellum to generation of vertical smooth eye movements. J Neurophysiol 48:75-99.

Chung S-H, Marzban H, Aldinger K, Dixit R, Millen K, Schuurmans C, Hawkes R (2011) Zac1 plays a key role in the development of specific neuronal subsets in the mouse cerebellum. Neural development 6:25.

Chung SH, Marzban H, Hawkes R (2009) Compartmentation of the cerebellar nuclei of the mouse. Neuroscience 161:123-138.

De Zeeuw CI, Chorev E, Devor A, Manor Y, Van Der Giessen RS, De Jeu MT, Hoogenraad CC, Bijman J, Ruigrok TJ, French P, Jaarsma D, Kistler WM, Meier C, Petrasch-Parwez E, Dermietzel R, Sohl G, Gueldenagel M, Willecke K, Yarom Y (2003) Deformation of network connectivity in the inferior olive of connexin 36-deficient mice is compensated by morphological and electrophysiological changes at the single neuron level. J Neurosci 23:4700-4711.

Delogu A, Sellers K, Zagoraiou L, Bocianowska-Zbrog A, Mandal S, Guimera J, Rubenstein JL, Sugden D, Jessell T, Lumsden A (2012) Subcortical visual shell nuclei targeted by ipRGCs develop from a Sox14+-GABAergic progenitor and require Sox14 to regulate daily activity rhythms. Neuron 75:648-662.

Dixon KJ, Hilber W, Speare S, Willson ML, Bower AJ, Sherrard RM (2005) Post-lesion transcommissural olivocerebellar reinnervation improves motor function following unilateral pedunculotomy in the neonatal rat. Exp Neurol 196:254-265.

Dom R, King S, Martin GF (1973) Evidence for two direct cerebello-olivary connections. Brain Res 57:498-501.

Fink AJ, Englund C, Daza RA, Pham D, Lau C, Nivison M, Kowalczyk T, Hevner RF (2006) Development of the deep cerebellar nuclei: transcription factors and cell migration from the rhombic lip. J Neurosci 26:3066-3076.

Geborek P, Jorntell H, Bengtsson F (2012) Stimulation within the cuneate nucleus suppresses synaptic activation of climbing fibers. Front Neural Circuits 6:120.

Giaquinta G, Casabona A, Smecca G, Bosco G, Perciavalle V (1999) Cortical control of cerebellar dentato‐rubral and dentato‐olivary neurons. Neuroreport 10:3009-3013.

Gilthorpe JD, Papantoniou EK, Chedotal A, Lumsden A, Wingate RJ (2002) The migration of cerebellar rhombic lip derivatives. Development 129:4719-4728.

Graybiel AM, Hartwieg EA (1974) Some afferent connections of the oculomotor complex in the cat: an experimental study with tracer techniques. Brain Res 81:543-551.

Green MJ, Wingate RJ (2014) Developmental origins of diversity in cerebellar output nuclei. Neural Dev 9:1.

Hargrave M, Karunaratne A, Cox L, Wood S, Koopman P, Yamada T (2000) The HMG box transcription factor gene Sox14 marks a novel subset of ventral interneurons and is regulated by sonic hedgehog. Dev Biol 219:142-153.

Hesslow G, Ivarsson M (1996) Inhibition of the inferior olive during conditioned responses in the decerebrate ferret. Exp Brain Res 110:36-46.

Highstein SM, Partsalis A, Arikan R (1997) Role of the Y-group of the vestibular nuclei and flocculus of the cerebellum in motor learning of the vertical vestibulo-ocular reflex. Prog Brain Res 114:383-397.

Hoshino M, Nakamura S, Mori K, Kawauchi T, Terao M, Nishimura YV, Fukuda A, Fuse T, Matsuo N, Sone M, Watanabe M, Bito H, Terashima T, Wright CV, Kawaguchi Y, Nakao K, Nabeshima Y (2005) Ptf1a, a bHLH transcriptional gene, defines GABAergic neuronal fates in cerebellum. Neuron 47:201-213.

Houck BD, Person AL (2014) Cerebellar Loops: A Review of the Nucleocortical Pathway. The Cerebellum 13:378-385.

Ito M (2013) Error detection and representation in the olivo-cerebellar system. Front Neural Circuits 7:1.

Jager P, Ye Z, Yu X, Zagoraiou L, Prekop HT, Partanen J, Jessell TM, Wisden W, Brickley SG, Delogu A (2016) Tectal-derived interneurons contribute to phasic and tonic inhibition in the visual thalamus. Nat Commun 7:13579.

Kim EJ, Battiste J, Nakagawa Y, Johnson JE (2008) Ascl1 (Mash1) lineage cells contribute to discrete cell populations in CNS architecture. Mol Cell Neurosci 38:595-606.

Kistler WM, De Jeu MT, Elgersma Y, Van Der Giessen RS, Hensbroek R, Luo C, Koekkoek SK, Hoogenraad CC, Hamers FP, Gueldenagel M, Sohl G, Willecke K, De Zeeuw CI (2002) Analysis of Cx36 knockout does not support tenet that olivary gap junctions are required for complex spike synchronization and normal motor performance. Ann N Y Acad Sci 978:391-404.

Lang EJ, Sugihara I, Llinás RR (1996) GABAergic modulation of complex spike activity by the cerebellar nucleoolivary pathway in rat. J Neurophysiol 76:255-275.

Lefler Y, Yarom Y, Uusisaari MY (2014) Cerebellar inhibitory input to the inferior olive decreases electrical coupling and blocks subthreshold oscillations. Neuron 81:1389-1400.

Legendre A, Courville J (1987) Origin and trajectory of the cerebello-olivary projection: an experimental study with radioactive and fluorescent tracers in the cat. Neuroscience 21:877-891.

Leznik E, Makarenko V, Llinás RR (2002) Electrotonically mediated oscillatory patterns in neuronal ensembles: an in vitro voltage-dependent dye-imaging study in the inferior olive. J Neurosci 22:2804-2815.

Llinás RR (2011) Cerebellar motor learning versus cerebellar motor timing: the climbing fibre story. J Physiol 589:3423-3432.

Llinás RR (2013) The olivo-cerebellar system: a key to understanding the functional significance of intrinsic oscillatory brain properties. Front Neural Circuits 7:96.

Long MA, Deans MR, Paul DL, Connors BW (2002) Rhythmicity without synchrony in the electrically uncoupled inferior olive. J Neurosci 22:10898-10905.

Lundell T, Zhou Q, Doughty M (2009) Neurogenin1 expression in cell lineages of the cerebellar cortex in embryonic and postnatal mice. Developmental Dynamics 238:3310-3325.

Machold R, Fishell G (2005) Math1 is expressed in temporally discrete pools of cerebellar rhombic-lip neural progenitors. Neuron 48:17-24.

Maricich SM, Herrup K (1999) Pax-2 expression defines a subset of GABAergic interneurons and their precursors in the developing murine cerebellum. J Neurobiol 41:281-294.

Martin GF, Henkel CK, King JS (1976) Cerebello-olivary fibers: their origin, course and distribution in the North American opossum. Exp Brain Res 24:219-236.

McClellan KM, Parker KL, Tobet S (2006) Development of the ventromedial nucleus of the hypothalamus. Frontiers in neuroendocrinology 27:193-209.

Medina JF, Nores WL, Mauk MD (2002) Inhibition of climbing fibres is a signal for the extinction of conditioned eyelid responses. Nature 416:330-333.

Morales D, Hatten ME (2006) Molecular markers of neuronal progenitors in the embryonic cerebellar anlage. J Neurosci 26:12226-12236.

Myat A, Henrique D, Ish-Horowicz D, Lewis J (1996) A chick homologue of Serrate and its relationship with Notch and Delta homologues during central neurogenesis. Dev Biol 174:233-247.

Najac M, Raman IM (2015a) Integration of Purkinje cell inhibition by cerebellar nucleo-olivary neurons. J Neurosci 35:544-549.

Najac M, Raman IM (2015b) Integration of Purkinje cell inhibition by cerebellar nucleo-olivary neurons. Journal of Neuroscience 35:544-549.

Schweighofer N, Lang EJ, Kawato M (2013) Role of the olivo-cerebellar complex in motor learning and control. Front Neural Circuits 7:94.

Sears LL, Steinmetz JE (1991) Dorsal accessory inferior olive activity diminishes during acquisition of the rabbit classically conditioned eyelid response. Brain Res 545:114-122.

Stanton GB (1980) Afferents to oculomotor nuclei from area "Y" in Macaca mulatta: an anterograde degeneration study. J Comp Neurol 192:377-385.

Steiger HJ, Buttner-Ennever JA (1979) Oculomotor nucleus afferents in the monkey demonstrated with horseradish peroxidase. Brain Res 160:1-15.

Sugihara I, Lohof AM, Letellier M, Mariani J, Sherrard RM (2003) Post-lesion transcommissural growth of olivary climbing fibres creates functional synaptic microzones. Eur J Neurosci 18:3027-3036.

Tolbert DL, Massopust LC, Murphy MG, Young PA (1976) The anatomical organization of the cerebello-olivary projection in the cat. J Comp Neurol 170:525-544.

Uusisaari M, Knöpfel T (2011) Functional classification of neurons in the mouse lateral cerebellar nuclei. The Cerebellum 10:637-646.

Uusisaari M, Obata K, Knöpfel T (2007) Morphological and electrophysiological properties of GABAergic and non-GABAergic cells in the deep cerebellar nuclei. Journal of neurophysiology 97:901-911.

Uusisaari MY, Knopfel T (2012) Diversity of neuronal elements and circuitry in the cerebellar nuclei. Cerebellum 11:420-421.

Van Der Giessen RS, Koekkoek SK, van Dorp S, De Gruijl JR, Cupido A, Khosrovani S, Dortland B, Wellershaus K, Degen J, Deuchars J, Fuchs EC, Monyer H, Willecke K, De Jeu MT, De Zeeuw CI (2008) Role of olivary electrical coupling in cerebellar motor learning. Neuron 58:599-612.

Vinueza Veloz MF, Zhou K, Bosman LW, Potters JW, Negrello M, Seepers RM, Strydis C, Koekkoek SK, De Zeeuw CI (2015) Cerebellar control of gait and interlimb coordination. Brain Struct Funct 220:3513-3536.

Wang VY, Rose MF, Zoghbi HY (2005) Math1 expression redefines the rhombic lip derivatives and reveals novel lineages within the brainstem and cerebellum. Neuron 48:31-43.

Yamamoto F, Sato Y, Kawasaki T (1986) The neuronal pathway from the flocculus to the oculomotor nucleus: an electrophysiological study of group y nucleus in cats. Brain Res 371:350-354.

Zordan P, Croci L, Hawkes R, Consalez GG (2008) Comparative analysis of proneural gene expression in the embryonic cerebellum. Dev Dyn 237:1726-1735.

FIGURE LEGENDS

FIGURE 1: SOX14 MARKS A SUBSET CELLS IN CEREBELLAR NUCLEI

A-D) P21 *Sox14*$^{Gfp/+}$ coronal sections showing the cerebellum from rostral to caudal. Only the lateral (Lat) cerebellar nucleus is seen in rostral sections (A). *Sox14*$^{+}$ cells are found in the cerebellar nucleus and these cells are distributed unevenly, seen clearly in the magnified image (Inset). B) The lateral nucleus merges with the interposed nuclei and the vestibular nuclei: superior vestibular nuclei (SuVe) and vestibulocerebellar nuclei (VeCb). There are *Sox14*$^{+}$ cells throughout, except in the dorsal parts of the medial nucleus. More caudally (C), the lateral and anterior interposed nuclei recede so to only occupy a small dorsolateral domain, while the posterior interposed (IntP) nucleus takes over. Small numbers of *Sox14*$^{+}$ cells are seen in the ventral edge of the medial nucleus (Inset). D) Most caudally, the medial (Med) nucleus is seen clearly as an almond shape above the posterior interposed (IntP) nucleus. Though the shape of the nucleus is well defined by the background staining, again, no *Sox14*$^{+}$ cells are seen in this region. Lat = lateral nucleus, LatPC = parvicellular lateral nucleus, IntDL = dorsolateral interposed nucleus, IntA= anterior interposed nucleus, IntP= posterior interposed nucleus, Med= Medial nucleus, VN= vestibular nucleus, RN= reticular nucleus. Scale bar, 200 µm.

FIGURE 2. IN THE CEREBELLAR NUCLEI SOX14 ARE SMALL, EXCLUSIVELY GABAERGIC, PV-VE NEURONS GFP VS PVALB, GANA CALB1,2, GABA, GAD1, GAD2

A-I) Comparison of Sox14:GFP with other known cell markers by immunohistochemistry or *in situ* hybridization in Sox14$^{Gfp/+}$ P21 sections (A, C-I) and primary cell culture of brain tissue from Sox14$^{Gfp/+}$ P0 neonates (B). Immunostaining for GABA (A&B), MAP2 (B), *Gad1* (C), *Gad2* (D), PValb (E), Calb1 (F) and Calb2 (G), imaged at 100x (40x for ISH) magnification of the lateral nucleus. The columns show the overlay, then GFP only and Alexa-568 only. The white arrowheads show examples of GFP^{+} cells that co-localise with GABA, *Gad1* and *Gad2*, but not PValb, Calb1 or Calb2. There is little immunoreactivity for Calb2 within the cerebellar nuclei (G), but a single GFP^{-}/Calb2^{+} cell is seen, denoted with an asterisk (*). H&I) In situ hybridisation against *PValb* (H), and

Calb2 (I) demonstrates the distribution of the different cell types. H) *PValb* expression is observed in complementary large, nuclear cells to GFP+ cells. I) *Calb2* expression is mostly observed in two distinct populations within the Sox14^{+} cells of the cerebellar nuclei. Sox14$^{–}$/*Calb2*$^{+}$ are seen in the central parts of the lateral nucleus, while Sox14^{+}/*Calb2*$^{+}$ exist in a dense cluster in the ventral parts of the lateral nucleus. Scatterplot (J) and histogram (K) of soma size as measured by mean soma diameter (μm). The mean soma diameters are as follows: GFP^{+}/Gad1 14.1 ± 0.3 μm; GFP$^{–}$/Gad1^{+} 15.1 ± 0.4 μm; and GFP$^{–}$/PValb^{+} 22.3 ± 0.3 μm (mean±SEM). The peak frequency for cell diameter of both GFP^{+} and GFP$^{–}$ *Gad1* populations are very similar. In addition, the larger GFP^{+} cells overlap with the *PValb*$^{+}$ population, demonstrating that size is not a sufficient determinant of cell type.

FIGURE 3: ANTEROGRADE LABELLING OF SOX14 PROJECTIONS IDENTIFIES TARGETS IN THE MIDBRAIN AND INFERIOR OLIVE

A-D) Unilateral injections of AAV-EF1a-DIO-mGFP targeted the lateral cerebellar nucleus (A) and projections were observed crossing the midline at the decussation of the superior cerebellar peduncle (xscp) (B) and terminating in the contralateral inferior olive (C) and the ipsilateral oculomotor nucleus (III). E-F) Bilateral injections of AAV-EF1a-DIO-mGFP and AAV-EF1a-DIO-TdTomato into the lateral cerebellar nucleus on either hemisphere show that axonal projections from each cerebellar hemisphere are bilateral, targeting both the ipsilateral and contralateral inferior olive though denser fluorescence is seen on the contralateral side (E). Although the projections clearly terminate in the contralateral olive, axons with synaptic boutons can be seen in the ipsilateral side contacting the same range of cells. Higher magnification view is shown in E'. F) High magnification shows mGFP expressing axons bypassing spaces where olivary cells reside shown by blue DAPI staining (asterisk, *). Scale bars: 20 μm (E', F), 200 μm (A, E), 500 μm (B, C, D).

FIGURE 4: RETROGRADE LABELLING IDENTIFIES DISTINCT SOX14 PROJECTION POPULATIONS

Injections of green RetroBeads into the ipsilateral oculomotor nucleus (A) and red RetroBeads into the contralateral inferior olive (B) of $Sox14^{Gfp/+}$ mouse. C) The cerebellar nucleus and surrounding regions. Scale 100 µm. Endogenous Sox14:GFP was stained with a far-red secondary antibody and shown in blue. Red RetroBeads were found in Sox14:GFP^{+} cells of the cerebellar nucleus, while green RetroBeads were only observed in the vestibular nuclei. The nucleus "Y" region of the vestibular nuclei contains Sox14:GFP^{+} cells that co-label with either green RetroBeads or red RetroBeads, but never both colours in one cell (C'). Unilateral injection of green RetroBeads into the inferior olive (D) of $Sox14^{Gfp/+}$ mouse at P19. E-F) Green RetroBeads were observed in the cerebellar nuclei only in cells that express Sox14:GFP (in magenta). The differential distribution of RetroBeads found in the contralateral and ipsilateral cerebellar nuclei (F) shows that projections to the inferior olive come from similar regions of both hemispheres but fewer cells contribute to the ipsilateral olive. G) Summary of *Sox14*$^{+}$ nucleo-olivary topography shown in AAV and RetroBead injections. The nucleo-olivary neurons of the lateral cerebellar nucleus (green) project to the principle olive and the dorsomedial cell group. The nucleo-olivary neurons of the interposed cerebellar nuclei (blue) project to the medial olivary nucleus and the dorsal olivary nucleus. The $Sox14^{+}$ neurons of the vestibular nuclei (red) project to the cap of Kooy of the medial nucleus and the ventrolateral protrusion. No $Sox14^{+}$ were observed from the medial cerebellar nucleus. All the projections were seen bilaterally in the inferior olive, but the contralateral contribution was consistently more intense (solid colour) compared to the ipsilateral contribution (stripe pattern). Scale bars: 20 µm (C'), 50 µm (A), 200 µm (B, D, F).

CN= cerebellar nucleus; III= oculomotor nucleus; IO= inferior olive; IntA= anterior interposed cerebellar nucleus; IntDL= dorsolateral interposed cerebellar nucleus; LatPC= parvicellular lateral cerebellar nucleus; Lat= lateral cerebellar nucleus; xscp= decussation of the superior cerebellar peduncle; mlf= medial longitudinal fascicle; Nuc Y= nucleus Y; IOA= inferior olive subnucleus A of medial nucleus; IOB= inferior olive subnucleus B of medial nucleus; IOBe= inferior olive beta

subnucleus; IOC= inferior olive subnucleus C of medial nucleus; IOD= inferior olive dorsal nucleus; IODdf= dorsal fold of the IOD; IODM= inferior olive dorsomedial cell group; IOK= inferior olive cap of Kooy of the medial nucleus; IOM= inferior olive medial nucleus; IOPr= inferior olive principal nucleus; IOVL= inferior olive ventrolateral protrusion.

FIGURE 5: INTEGRATION OF INHIBITORY PROJECTION NEURONS INTO THE NUCLEI IS MEDIATED BY SOX14

A) $Sox14^{Gfp/+}$ hindbrains were opened up dorsally along the midline and mounted flat so the rhombic lip, which originally lined the intersection between the cerebellum and roof plate, is the most lateral edge (in green), while the cerebellar anlage is in orange. GFP expression is seen at E11.5 (B) and E12.5 (C) on either side of the midline, while expression in the cerebellar plate is only seen from E12.5 onwards. D&E) BrdU birth dating analysis. Scale 20 µm. GFP^+ cells co-localise with BrdU that was injected at E10. 5 (D), while BrdU injected at 12.5 (E) shows no co-localisation, showing all the GFP^+ cells are born before E12.5. F) IHC against Lhx1/5 and GFP in the $Sox14^{Gfp/+}$ E12.5 sagittal brain sections. The Lhx1/5 expressing cells span the anterior-posterior axis of the cortical transitory zone, and are mostly Purkinje cell precursors. However, there is a dorsal layer of $Lhx1/5^+$ and GFP^+ population that are genetically distinct, seen in the higher magnification images (inset). These cells appear to be in a tangential orientation (white arrowheads), unlike the $GFP^-/Lhx1/5^+$ Purkinje cells which are migrating radially from the ventricular zone. G) $Pax6^+$ cells migrating along the rhombic lip migratory stream towards the nuclear transitory zone sit dorsal to the GFP^+ cells. H) A schematic to show the tangential orientation of the GFP^+ cells, seen in green, alongside the Pax6 excitatory cells migrating tangentially along the subpial rhombic lip migratory stream (RLS) in red, and the $GFP^-/Lhx1/5^+$ Purkinje cells that are migrating radially from the ventricular zone. I-J) Coronal sections of the $Sox14^+$ cells in the developing CN of P0 $Sox14^{Gfp/+}$ mouse (I) compared to the $Sox14^{Gfp/Gfp}$ knock-out mouse (J). Scale 200 µm. I' shows the same image without drawn borders to highlight that for the $Sox14^{Gfp/+}$ mouse, the migratory streams already resemble the future boundaries between the sub-nuclei, while for the knock-out, the cells fail to populate some areas, leaving large gaps

(marked by *) and deviant clusters of cells. There are still some likenesses between the two brains, which suggests that there are other migratory mechanisms at work in the development of nucleo-olivary neurons. Density of vGAT labelling in the IO od an adult wildtype (K) and Sox14 mutant (L) mouse show a difference in signal to background intensity (M). Scale bars: 100 μm (F), 200 μm (I-L).

FIGURE 6: TARGETED ABLATION OF SOX14 NEURONS LEADS TO LOCOMOTOR DYSFUNCTION

Assessment using *Gad1* labelling as a measure of nucleo-olivary cell loss. The schematic represents the average density of *Gad1* reactive cells in the sham injected mice (A), all the $Sox14^{Cre/+}$ experimental mice (B), and selected averaged data for the 6 experimental mice that showed extensive cell loss (more than 70%) compared to sham (C). D) Rotarod data for all experimental mice against the sham injected group. The experimental mice show significantly reduced latencies for both day 2 ($p=0.0324$) and day3 ($p=0.0374$). E) Rotarod data for the 6 selected experimental mice shown in C against the sham injected group. The selected group perform worse with significantly reduced latencies for both day 2 ($p=0.041$) and day3 ($p=0.036$). Mean ± SEM. Two-way ANOVA followed by Bonferroni post-tests: main effect of trial time, $F(2,120) = 1122$, $P < 0.0001$; main effect of ablation, $F(1,120) = 4.479$, $P = 0.0064$; ablation × trial time interaction, $F(2,1.20) = 1.25$, $P = 0.2903$). F) Percentage of missteps measured on the introduction onto the Erasmus ladder apparatus shows the experimental group initially made more mistakes compared to the sham group. Median percentage of missteps in sham and experimental groups were 11.85 and 19.26%, thus the distributions in the two groups differed significantly (Mann-Whitney $U = 23$, $n_1 = 10$ $n_2 = 10$, $p = 0.0433$ two-tailed). Median with 95%Cl.

G) The various types of steps that are measured, image adapted from Noldus. The mouse ordinarily prefers to travel along the top set of rungs (green) and can perform short, long or jump steps according to how many rungs are skipped between steps. The mouse may also take back steps, moving backwards against the tailwind, or perform a misstep, where a mistake leads the mouse to step onto a lower set of rungs (blue). During associative learning trials, an obstacle rung (orange)

may swing up to obstruct the path of the mouse so that it must step over the rung. While the placement of the obstacle rung may change between trials, the post-perturbation step-time is defined as the time between activation of the rung before the obstacle to the rung after the obstacle, and is a measure of how adapted . (H-J) Usage of various step types over the training days (Day1-4). H) The percentage of steps that were long steps used in each trial day. The effect of trial days was extremely significant ($p< 0.0001$, $F(3,80)=36.32$). I) The percentage of steps that were back-steps used in each trial day. The effect of trial days was extremely significant ($p< 0.0001$, $F(3,80)=9.27$). J) The percentage of steps that were jumps used in each trial day. The effect of ablative injection was significant, showing a decreased percentage of jumps in the experimental animals compared to sham (adjusted $p=0.0033$, $F (1, 80) = 9.20$, Two-way ANOVA Corrected method of Benjamini and Yekutieli). Mean ± SEM. K) Post-perturbation step-times in the different associative learning trials. During the first 4 days, only undisturbed trials were run to train the mice to traverse the ladder. Since there is no obstacle in these trials, there is the post-perturbation step-time is the average step-time for a normal step (black). On days 5-8, trials are run so that the mouse is presented with either CS only (green), US only (orange) or paired CS-US (purple) stimuli. Where there is an obstacle presented in the trial, the post perturbation step-time will increase if the mouse is not anticipating the obstacle. In all trial types, there was no significant difference in post-perturbation step-time between the two groups. Mean ± SEM.

Figure 1: Prekop et al.

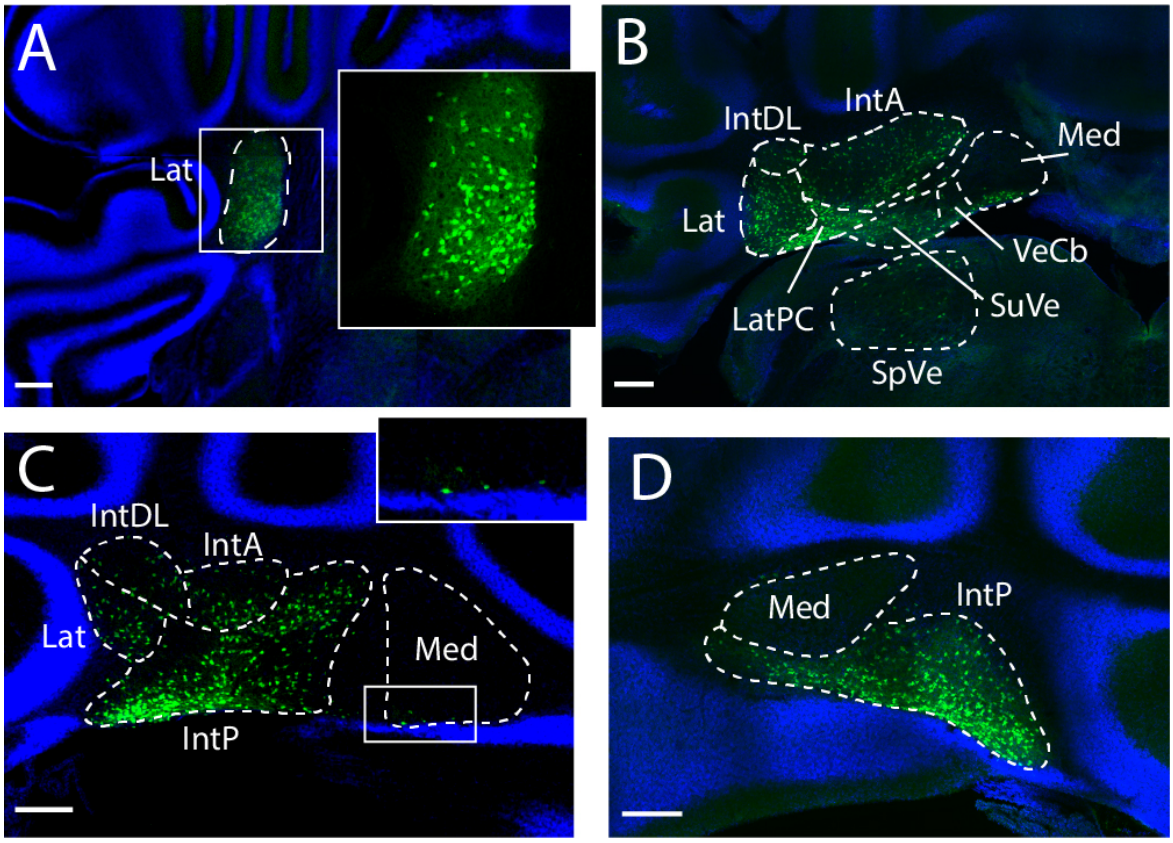

Figure 2: Prekop et al.

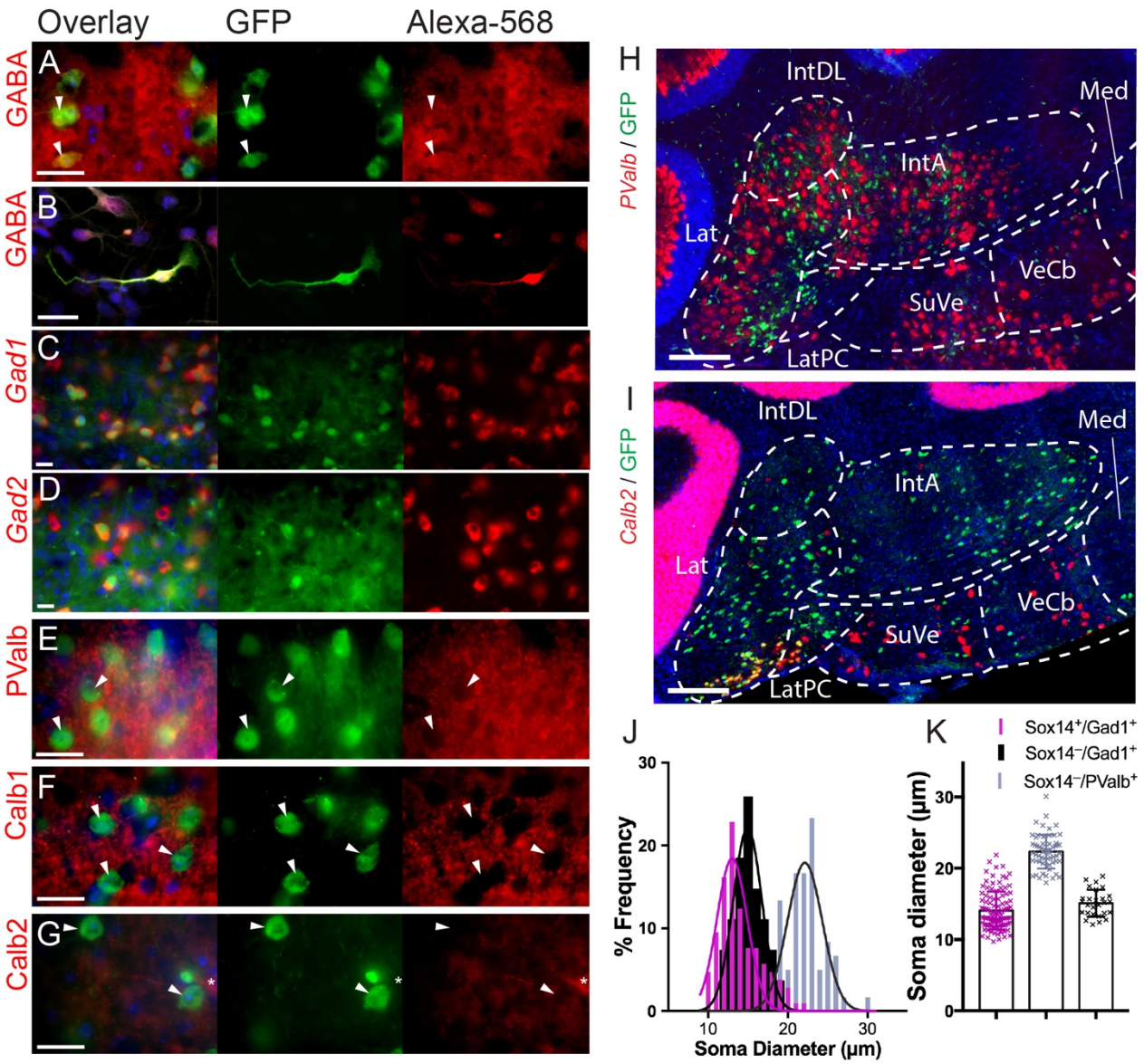

Figure 3: Prekop et al.

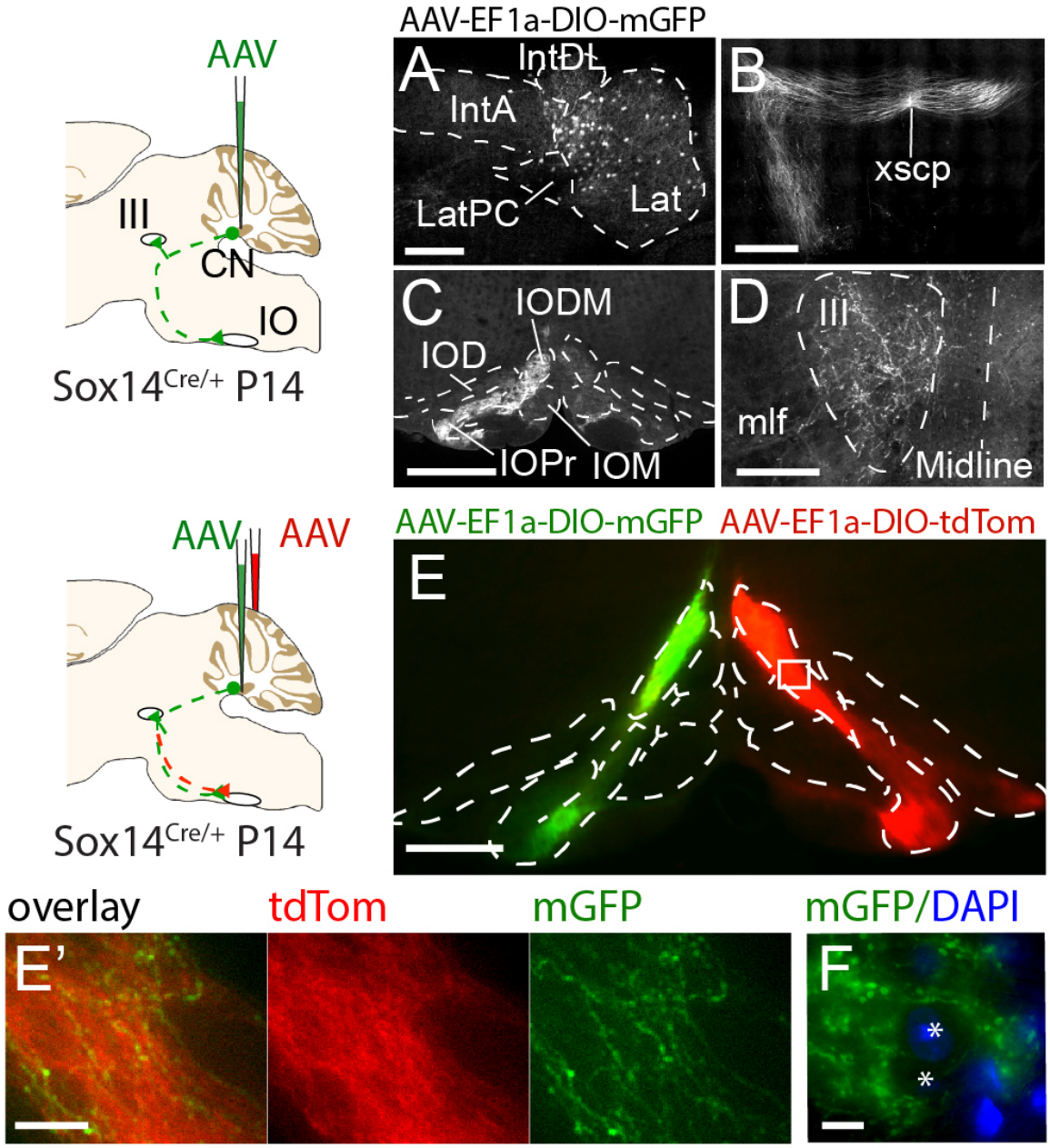

Figure 4: Prekop et al.

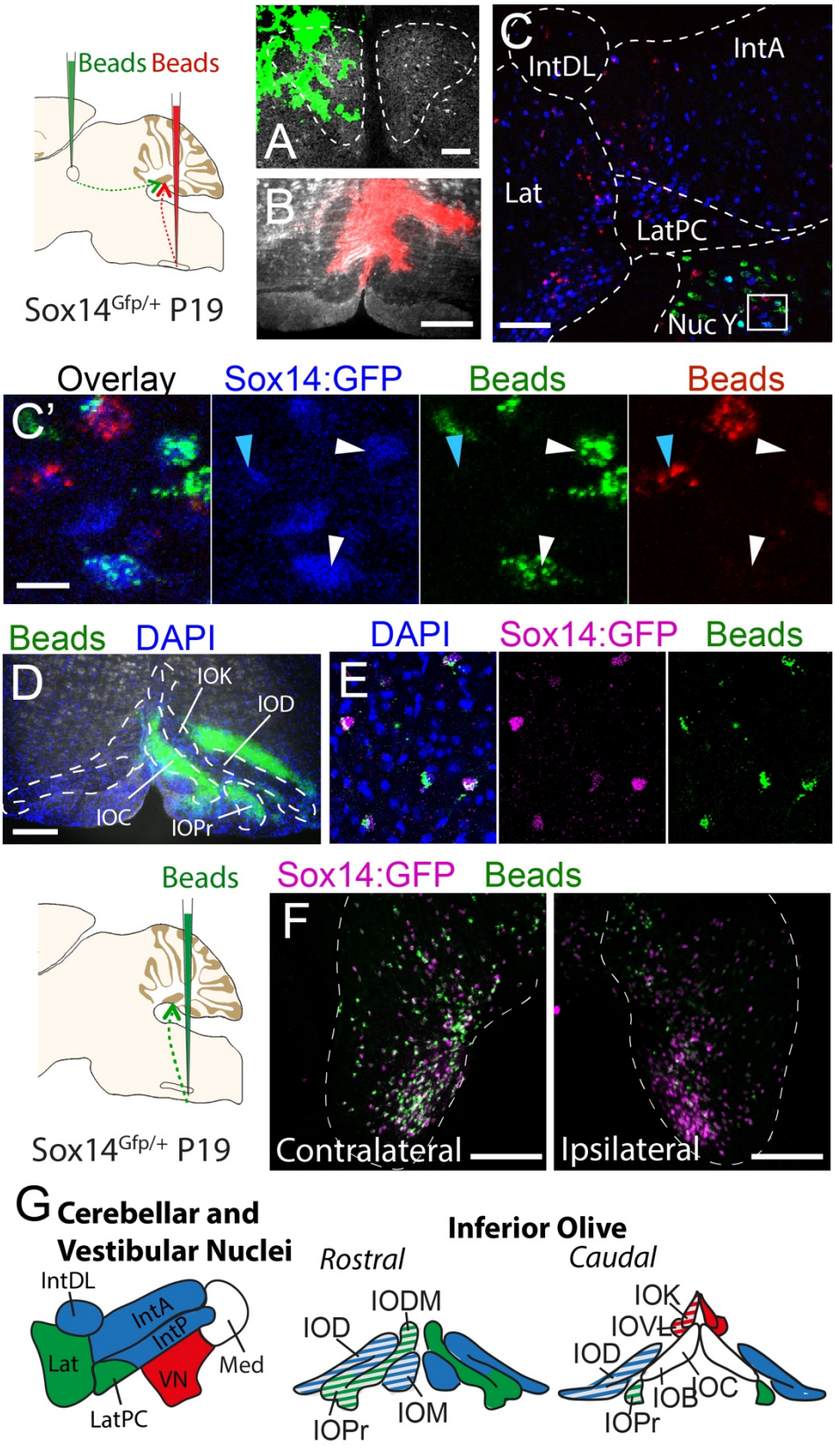

Figure 5: Prekop et al.

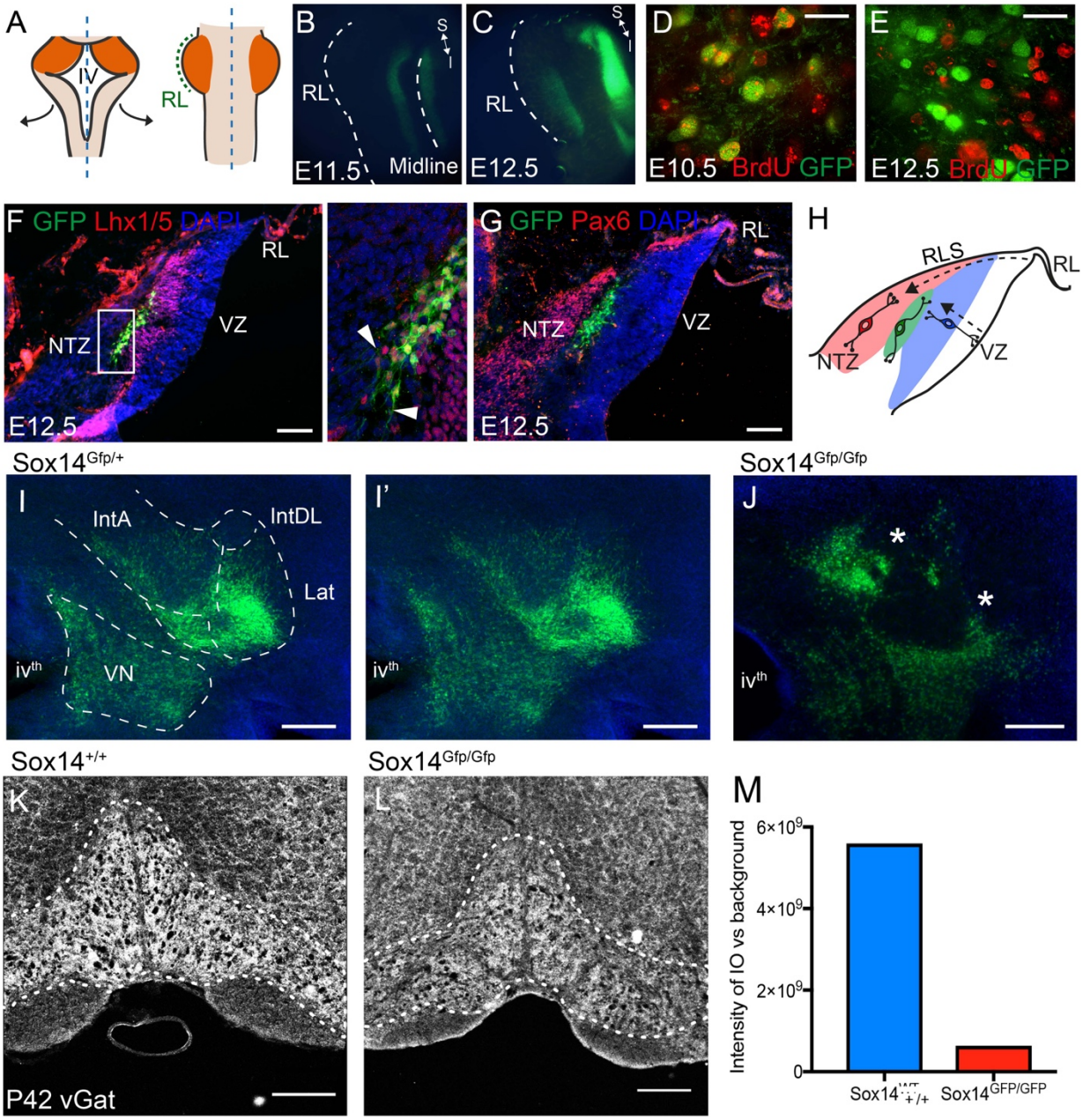

Figure 6: Prekop et al.